Dispersion Characteristics of Optically Excited Coplanar Striplines: Pulse Propagation

D. S. PHATAK AND A. P. DEFONZO SENIOR MEMBER, IEEE

Abstract—**This paper analyzes the propagation of optically excited picosecond electrical pulses on coplanar striplines. A full-wave analysis method that includes dispersion and losses over terahertz bandwidths is outlined. Results of the full-wave analysis are interpreted in terms of the underlying physical phenomena. The full-wave analysis reveals the existence of peaks in the dispersion curve of the coplanar stripline. These are interpreted in terms of the onset and coupling of the substrate modes to the transmission line mode. Results of the full-wave analysis are in good agreement with those obtained by established theory. Pulse propagation is simulated using the dispersion and loss data obtained from the analysis and accounts for all the relevant mechanisms. Results of simulations are compared with experimental data available in the literature for normal as well as superconducting lines. It is demonstrated that the superconducting phenomena are not dominant, whereas modal dispersion and substrate losses dominate the evolution of the output pulse and must be included for accurate modeling of pulse propagation on coplanar striplines**

I. Introduction

CONTINUED progress in millimeter-wave integrated circuits, high-speed digital circuits, and switching devices has necessitated the development of systems capable of handling the increasing signal bandwidths. One of the key issues which must be addressed is the dispersion of ultrafast signals traveling on the guiding structures used to interconnect devices in high-speed circuits. This phenomenon leads to distortion of the spectral and temporal characteristics of the propagated signal, considerably limiting the usable bandwidth. Although generally associated with performance degradation, this phenomenon may have practical benefits, including dispersion compensation of optically transmitted microwave signals. One way to characterize the transient and broadband response of transmission lines is to use optical pulse excitation. Optical excitation is important for metrology, and also as an innovative interconnect technology.

Researchers have analyzed various aspects of this problem. Pulse propagation on microstrips and coplanar striplines has been investigated [1], [2], where the frequency-dependent propagation velocity has been used to find the temporal spread of the output waveform. Various sampling techniques have been used [3]–[6] to measure the waveforms. Transmission on superconducting lines has also been studied, and a general model for analyzing pulse propagation has been developed [7]. These pulse propagation models, however, are not complete. The analysis of [1] and [2], for instance, ignores all losses while the development in [7] leaves out substrate losses due to radiation and surface waves. Such losses have been measured as a function of frequency and a theory based on reciprocity has been developed to estimate them [8], [9].

In this paper we take into account all the phenomena relevant to pulse propagation on coplanar striplines (CPS's) and for the first time demonstrate the effects of substrate losses on pulse propagation. In Section II, we give a physical description of pulse propagation on the CPS and determine the relevant parameters of the CPS. Here, we present the results of the full computation of waveguide dispersion *and losses*. The full-wave analysis reveals new features such as the existence of peaks in the dispersion curve of a coplanar stripline. These are interpreted in terms of the underlying physical phenomena, viz. the onset and coupling of substrate modes to the transmission line mode. The results of the full-wave analysis are compared with empirical and closed-form expressions available in the literature. A detailed mathematical formulation will be presented in a separate paper [10]. Section III presents a simulation of pulse propagation based on the results of the foregoing analysis. The simulation outputs are compared with experimental data published in the literature.

II. Parameters of the Coplanar Strip Transmission Line

A schematic diagram of pulse propagation is shown in Fig. 1(a). The pulses are launched on the line and are then sampled at suitable distances to monitor attenuation and spread. The hatched cone in Fig. 1(a) indicates merely the direction of radiation in the substrate and does not mean that the radiation precedes the pulse. The CPS geometry is as shown in Fig. 1(b). CPS with infinite thickness substrate is a special case of this geometry with

Manuscript received August 2, 1989; revised November 17, 1989. This work was supported by the Air Force Office of Scientific Research under Grant AFOSR-88-0106.

The authors are with the Electrical and Computer Engineering Department, University of Massachusetts, Amherst, MA 01003.

IEEE Log Number 9034818.

0018-9480/90/0500-0654$01.00 ©1990 IEEE

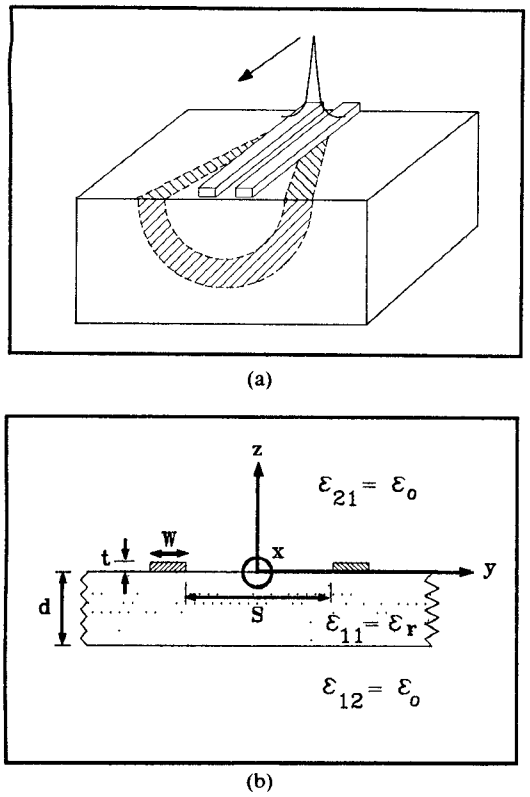

Fig. 1. The coplanar stripline (CPS) geometry. (a) Pulse propagation schematic. (b) Cross section of the CPS on a finite-thickness substrate.

$d = \infty$. The parameters needed for pulse propagation computations are the real and imaginary parts of the propagation constant. These correspond to dispersion and losses, respectively. The dominant dispersion mechanisms are waveguide dispersion and dispersion due to metallic conductors. The dispersion contributed by lossy dielectric substrate can be neglected. Loss mechanisms considered here are substrate losses, conductor losses, and dielectric material losses. Coplanar striplines on infinitely thick substrate lose energy to radiation into the substrate, while lines on a finite thickness substrate lose energy to guided modes of the substrate when the transmission line mode propagates faster than substrate modes [8], [9]. We use the generic term *substrate losses* (a term distinct from the dielectric material loss of the substrate) to refer to these losses. This leakage occurs above a critical frequency, at which point the dispersion curve of the substrate mode crosses that of the transmission line. At the frequency of operation, the radiation occurs around an angle ψ given by the phase match condition

$$\cos \Psi = \frac{\text{propagation constant of the transmission line mode}}{\text{propagation constant of substrate mode}}. \tag{1}$$

More recently, leakage to such modes has been reported by Oliner *et al.* for a microstrip line on an anisotropic substrate [11]. It is believed that the above physical phenomenon, viz. the transmission line mode traveling faster than the substrate mode, also accounts for the leakage effects observed by Oliner *et al.* [10].

A. Dispersion

Full-wave analyses [12], [13] and semiempirical techniques [14], [15] have been employed to find the frequency-dependent propagation constant of the microstrip. An approximate expression has been derived through curve fitting the exact analysis [16] and extended to the dispersion data of coplanar waveguide [2] to give

$$\sqrt{\epsilon_{\text{eff}}(f)} = \sqrt{\epsilon_{\text{eff}}(0)} + \left[\frac{\sqrt{\epsilon_{\text{eff}}(\infty)} - \sqrt{\epsilon_{\text{eff}}(0)}}{1 + \alpha G^{-b}}\right],$$
$$\epsilon_{\text{eff}}(\infty) \approx \epsilon_r \tag{2}$$

where $\epsilon_{\text{eff}}(0)$ is the quasi-static value and has been estimated in literature [17, eq. (7.18)]. $G = f/f_{\text{TE}}$ is the normalized frequency, where $f_{\text{TE}} = c/(4h\sqrt{\epsilon_r - 1})$ is the cutoff frequency above which the first non-TEM mode enters the microstrip. The dispersion curve for the coplanar stripline has a similar shape; hence the above expression can be used to approximate that curve as well. For a CPS on a substrate of infinite thickness, however, f_{TE} is not defined. This difficulty can be circumvented by setting

$$\alpha G^{-b} = af^{-b}$$

i.e.

$$\alpha \cdot f_{\text{TE}}^{b} = a \tag{3}$$

where f is the frequency. The above modification thus incorporates both finite-thickness and infinite-thickness substrates and has been employed in our work.

A full-wave analysis of the coplanar stripline was carried out and the data generated were fitted to (2) and (3). The results are as shown in Fig. 2(a). Peaks are observed in the dispersion curve at places where a substrate mode dispersion curve crosses that of a transmission line mode [10]. These peaks are attributed to the coupling of the transmission line mode to the substrate modes. It can be shown that the poles of the Green's functions (relating transverse currents on the $z = 0$ plane to the fields) correspond to substrate modes (i.e., TE and TM) modes of the dielectric slab waveguide [10]. Mathematically, the phase match condition for excitation of substrate modes is reflected in the fact that the pole corresponding to a substrate mode is encountered in the reaction integrals only if its propagation constant exceeds that of the transmission line mode at the frequency of operation. Under certain conditions these poles are of second order and are not simple poles, as is commonly believed [10]. When the phase match condition is met in the forward direction (i.e., ψ in (1) is zero), a substrate mode copropagates with the transmission line mode in the $+x$ direction. In this case, the corresponding pole is of second order. The reaction integrals, however, also contain expansion functions that contribute a zero of second order, which cancels the double pole contributed by Green's function, and

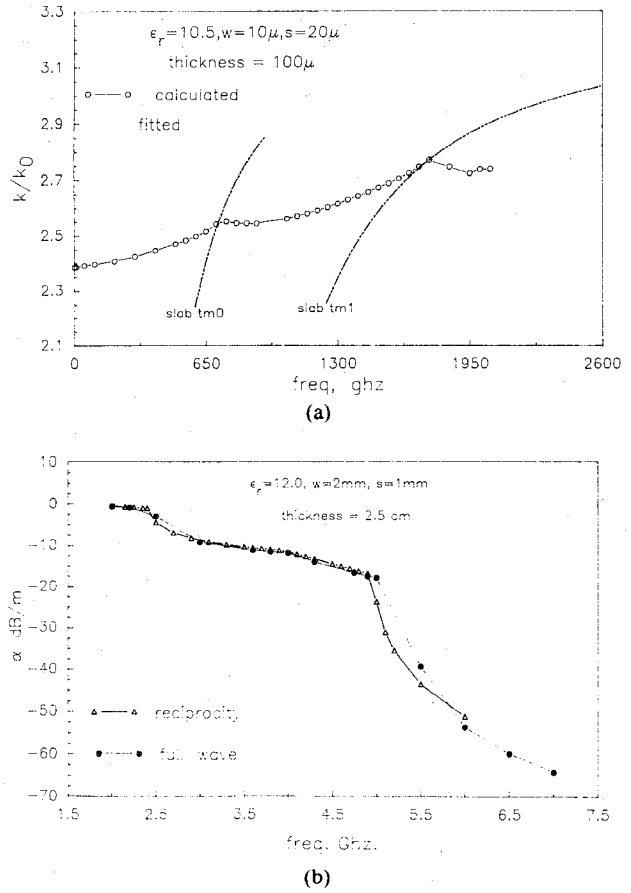

Fig. 2. Waveguide dispersion and substrate mode loss as functions of frequency. (a) Waveguide dispersion (normalized to k_0) versus frequency for coplanar striplines with $d \approx 10w$. Also shown is the curve fitted to eqs. (2) and (3). Dispersion curves for TM_0 and TM_1 slab modes are superimposed. (b) Comparison of substrate mode losses obtained by full-wave analysis and by reciprocity.

renders it a removable singularity [10]. Physically, the zero of the current expansion function transform is caused by an odd current distribution of the dominant mode of the CPS. Such a current distribution cannot support a single TM to z slab mode propagating in the x direction. It can, however, support a superposition of such modes that results in the proper symmetry, to give rise to a radiation pattern similar to the one illustrated in Fig. 1(a). Thus the symmetries of the currents and fields affect which of the substrate modes can be excited.

In Fig. 2(a) the peaks appear only at the crossings of TM-type substrate modes because the transverse current is negligibly small compared to the longitudinal current for the line dimensions considered there. When wider lines are used in the computation, additional peaks are observed at crossings of TE-type modes [10]. It is expected that coupling to substrate modes will be stronger when substrate thickness is approximately the same as the line dimensions. This is borne out by the dispersion plot of Fig. 7(a). The dispersion data available in the literature do not show peaks. The empirical fits generated by using (2) and (3) smooth out the peaks and therefore lack the sharp features. The effect of these features on the pulse dispersion is considered in the next section.

Dispersion due to metal conductors can be estimated as

$$\beta_{\text{cond}} = \text{Im}\left[\frac{Z_s}{Z_0}\right] g$$

$$g = 17.34 \cdot \frac{P'}{\pi s} \cdot \left(1 + \frac{w}{s}\right) \cdot \left\{ \frac{\frac{1.25}{\pi} \ln\left(\frac{4\pi w}{d}\right) + 1 + \frac{1.25d}{\pi w}}{\left[1 + 2\frac{w}{s} + \frac{1.25d}{\pi s} \cdot \left(1 + \ln\frac{4\pi w}{d}\right)\right]^2} \right\} \quad (4)$$

where Z_s is the frequency-dependent complex surface impedance, Z_0 is the quasi-static impedance, and g is a geometry factor. Further details can be found in [17].

Waveguide dispersion is about an order of magnitude larger than metal dispersion and dominates the total dispersion. Hence, error in the estimation of metal dispersion has negligible effect on the total dispersion. The above model for metal dispersion, although approximate, is sufficient for our purposes.

B. Losses

At the frequencies of interest, the line is lossy. Dielectric loss, metal loss, and radiation/surface wave loss are considered here. The substrate losses have been evaluated by a theory based on reciprocity [8], [9]. There, it is shown that radiation losses in the air region above the line are negligible. Modified versions of those loss expressions have been employed in our work. These losses are given by

$$\alpha_{\text{rad}} = (3 - \sqrt{8}) \frac{\pi^4}{4} \sqrt{\frac{\epsilon_{\text{eff}}}{\epsilon_r}} \frac{\sin^4 \Psi}{KK'} \frac{w^2}{\lambda_d^3} \quad (5)$$

$$\alpha_{\text{sw TE}} = \frac{\pi^4}{2\sqrt{2}} \frac{\sqrt{1 + 1/\epsilon_r}}{h_e K' K} \sin^3 \Psi \sin\theta_d \cos^2 \phi_{\text{TE}} \left(\frac{w}{\lambda_d}\right)^2 \quad (6)$$

$$\alpha_{\text{sw TM}} = \frac{\pi^4}{2\sqrt{2}} \frac{\sqrt{1 + 1/\epsilon_r}}{h_e K' K} \cdot \sin\Psi \cos^2\Psi \sin\theta_d \cos^2\theta_d \sin^2\phi_{\text{TM}} \left(\frac{w}{\lambda_d}\right)^2. \quad (7)$$

The notation used here is the same as that in the above-mentioned references. However, frequency-dependent values of ϵ_{eff} have been used here instead of the quasi-static value. Also, a few errors in some of the prefactors have been corrected.

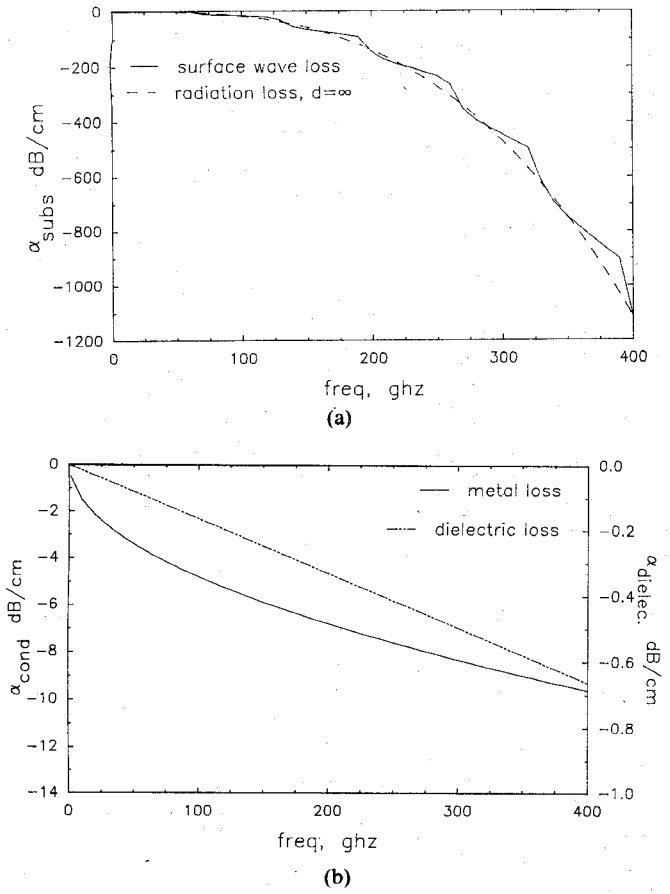

Fig. 3. Losses for a CPS with $\epsilon_r = 43$, $w = 50$ μm, $s = 50$ μm, and $d = 500$ μm over the frequency range spanned by the input pulse in Fig. 5(a). (a) Surface wave loss for a substrate having a thickness $d = 500$ μm and radiation loss for $d = \infty$. (b) Conductor and dielectric losses.

The dielectric and conductor losses are given by

$$\alpha_{\text{dielec}} = 27.3 \frac{\epsilon_r(\epsilon_{\text{qstat}} - 1)\tan\delta}{\sqrt{\epsilon_{\text{qstat}}}(\epsilon_r - 1)\lambda_0} \quad \text{dB/unit length}$$

$$\alpha_{\text{cond}} = \text{Re}\left[\frac{Z_s}{Z_0}\right] g \quad \text{dB/unit length} \tag{8}$$

respectively, where the geometry factor g is given by (4). Further details on the loss expressions can be found in [17]. There are many models of conductor losses. Depending on surface roughness and other factors, more elaborate theories may be necessary. Also, the accuracy of the dielectric loss model has not been established. The above models, however, are sufficient for our purposes, since these losses turn out to be much smaller than surface wave loss in the frequency range of interest.

Losses given by (5)–(8) are added to obtain $\text{Im}(k_x)$ (i.e., the total attenuation per unit length). Such a method implicitly assumes that the real part of the propagation constant can be evaluated independently of the imaginary part. This assumption has to be verified along with the accuracy of the above loss expressions. Such an error assessment is essential for the substrate losses since they dominate the total attenuation. To this end, a full-wave analysis including the dielectric and substrate losses was carried out by extending the method of [18]. The lossy nature of the metal, however, was not incorporated in the full-wave analysis, and the boundary condition $E_{\tan} = 0$ on perfect conductors was applied to the strip conductors. A sample result of this computation is shown in Fig. 2(b). Also plotted in the figure is the substrate loss curve computed by reciprocity based on expressions (5)–(8). The agreement is good. Moreover, the values of the real part of the propagation vector as given by this full-wave computation are essentially the same as those obtained by the full-wave analysis with *losses excluded* [10]. This shows that the real part of the propagation vector can be treated independently of these losses *over the frequency range and line dimensions under consideration*. It also shows that losses can be considered additive [10]. Thus the full-wave analysis demonstrates that expressions (5)–(8) are sufficiently accurate to model losses for pulse propagation computations.

The frequency range of interest spanned by the pulses typically used in the propagation experiments is roughly up to 400 GHz. For this frequency range, losses for a CPS with $\epsilon_r = 43$, $w = s = 50$ μm, and thickness $= 500$ μm, computed using expressions (5)–(8), are shown in Fig. 3. Part (a) shows the radiation loss and part (b) shows conductor and dielectric losses. It is evident that the substrate losses are substantially higher than metal or dielectric losses.

III. Pulse Propagation Model and Results

The method used to analyze the pulse propagation is superposition:

$$V(\tau, z) = \mathcal{F}^{-1}\left[\mathcal{F}\{V(\tau, 0)\} \cdot e^{-\gamma(f)z}\right] \tag{9}$$

where $\mathcal{F}$ denotes the Fourier transform. The input pulse is Fourier decomposed into its frequency components. Each component is then propagated to the given distance z with its characteristic propagation factor $\gamma(f)$, which includes dispersion and losses. Finally, all the frequency components are reassembled via an inverse Fourier transform to obtain the propagated pulse waveform. The real part of $\gamma(f)$, which accounts for dispersion, and the imaginary part, which accounts for losses, have to be computed at all the frequency components in the pulse. In the computer programs we use IMSL routines to do the forward and reverse transforms. For accuracy, we use a sufficiently large number (1024) of sample points for computing the transforms. The full-wave analysis is extremely computation intensive, and requires about 30 min of CPU time on a VAX-11/780 machine to evaluate $\gamma(f)$ at one frequency. Therefore, a full-wave analysis cannot be performed *on line* at each of the frequency samples in the discrete Fourier transform of the pulse. Moreover the loss expressions (5)–(8) are accurate enough to replace the full-wave computation. Also, these are simple and can be evaluated *on line* at each of the frequency samples. The waveguide dispersion, however, cannot be approximated by simple closed-form expressions because of peaks. In view of this, our strategy is to compute the waveguide

dispersion contribution to $\gamma(f)$ beforehand. The data points are computed with sufficient resolution to allow accurate linear interpolation for frequency samples that fall within the range of computed data. This linear interpolation is essential in order to include the effects of the peaks of the dispersion curve in the simulation. At high frequencies many more modes are encountered and the peaks come closer together but individual peaks are not so prominent. In this limit, the full-wave computation of ϵ_{eff} becomes increasingly time consuming. Hence, we compute data points only up to a maximum frequency. This frequency is determined by the lower of the two values: (i) where eight poles are encountered or (ii) where $\lambda_d \approx (w/3)$. Beyond this point, the number of expansion modes needed for a convergent solution is large and the moment method solution is not practical. In this region, empirical expressions are used to extrapolate the waveguide dispersion data. These expressions are obtained by curve fitting constants a and b in (2) and (3) to the data *computed by full-wave analysis*, and adequately describe the shape of the dispersion curve in the asymptotic region. Metal dispersion, all losses, and the attenuation coefficient are computed on line at each frequency in the discrete Fourier transform, since these terms are easy to evaluate.

The results of the simulation are shown in Figs. 4–7. All the plots titled "measured" in our figures have been obtained by digitizing the waveforms published in the literature. Line dimensions and all other relevant parameters are also taken from published data. In Fig. 4, we simulate the propagation of pulses measured in [19]. The maximum amplitude of the digitized data is normalized to unity to obtain the input pulse. Fig. 4(a) compares the measured waveform to the simulated one, at low temperatures, with metal conductivity $\sigma = 4.8\times10^8$ mho/m. Fig. 4(b) compares the measured and simulated waveforms for room temperature propagation with $\sigma = 4.0\times10^7$ mho/m. The delay and general shape of the simulated output agree well with the measured waveforms. The loss models of (7) and (8) slightly underestimate the substrate loss and overestimate the metal loss compared with the values obtained in [19].

In Fig. 5 we simulate propagation of the experimentally measured input pulses in [7]. It should be noted that the time values here are not absolute times with respect to the launched pulse, as in the previous figure. Instead, they represent time *in an interval*, which is suitably chosen to capture most of the propagated pulse waveform, including the rising and falling edges. The shape, spread, and other characteristics of measured waveforms are properly reproduced by the simulations. The data in [7], however, do not give measured values of the field amplitudes. Therefore, one can only compare the shape and qualitative features of the output pulse. Fig. 5(a) shows the measured waveforms. Fig. 5(b) shows the simulated output including surface wave losses, and Fig. 5(c) shows the output without surface wave losses. In the computations of Fig. 5(b) we do not account for the superconducting dispersion or loss, yet all the qualitative features of the measured output are reproduced by the simulation. The exclusion of surface wave losses does lead to more ringing and higher pulse amplitudes, as expected, since the surface wave loss rapidly depletes the higher frequencies. This output suggests that superconducting dispersion or loss is not a dominant mechanism for these lines at the frequencies contained in these pulses. It also shows that radiation loss does not have significant effects on output pulse shape at the propagation distances shown in that figure. To see the effects of radiation, shorter pulses have to be propagated over much longer distances on lines with thicker substrates [19], [20].

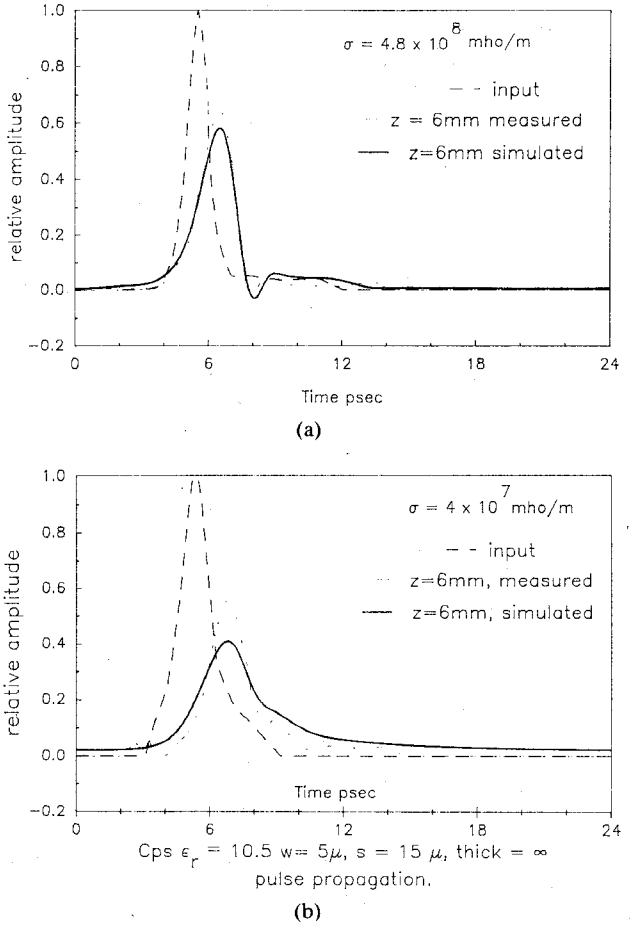

Fig. 4. Simulation of pulse propagation data from [19]. (a) Cooled lines. (b) Lines at room temperature.

Fig. 6 simulates the pulse propagation data reported in [21]. Fig. 6(a) shows the input pulse. Once again, the time axes in parts (b) and (c) of the figure are not absolute delays with respect to the times in part (a) but represent *intervals* chosen to capture the propagated pulse waveforms. Fig. 6(b) shows the pulse propagated on gold lines. In the simulation, we have used a conductivity value of $\approx 5\times10^8$ mho/m for gold at 10 K. The agreement with measured data is excellent. Fig. 6(c) shows the same pulse propagated on superconducting YBCO lines. Here again our analysis does not include any superconducting dispersion or losses. To approximate the low-loss behavior in

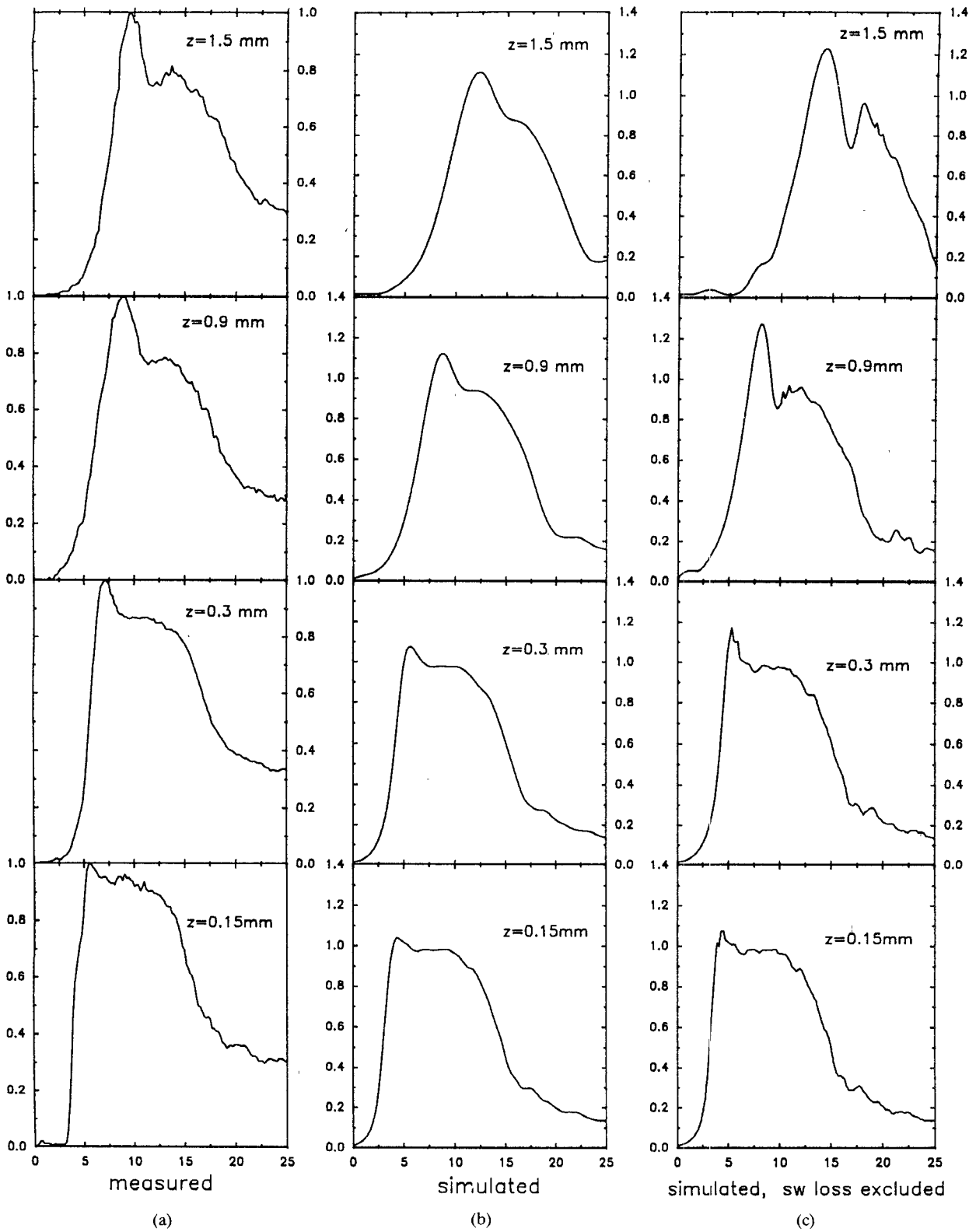

Fig. 5. Simulation of pulse propagation on a CPS with a finite-thickness substrate having $w = 50$ μm, $s = 50$ μm, and $d = 500$ μm. (a) Measured (from [7]). (b) Simulated. (c) Simulated excluding surface wave losses.

the superconducting state, we used conductivity values 10 and 100 times that of cooled gold for the simulations plotted in Fig. 6(c). The simulated outputs are almost identical despite an order-of-magnitude difference in conductivity values. This again suggests that metallic losses or dispersion do not significantly influence the output pulse waveform. Radiation losses and modal dispersion are the dominant mechanisms. The good agreement with measured data despite exclusion of any superconducting phenomena again suggests that the superconducting effects do not dominate pulse propagation on the lines under consideration.

Finally, to see the effect of dispersion peaks on pulse propagation we simulate the propagation on a CPS with

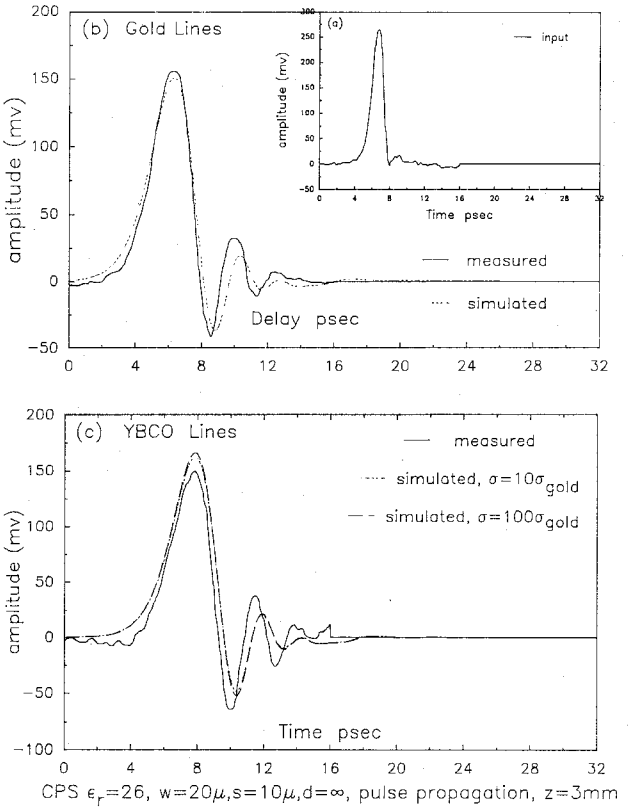

Fig. 6. Simulation of pulse propagation data from [21]. (a) Input pulse. (b) Measured and simulated output for propagation on gold lines. (c) Measured and simulated output for propagation on YBCO lines.

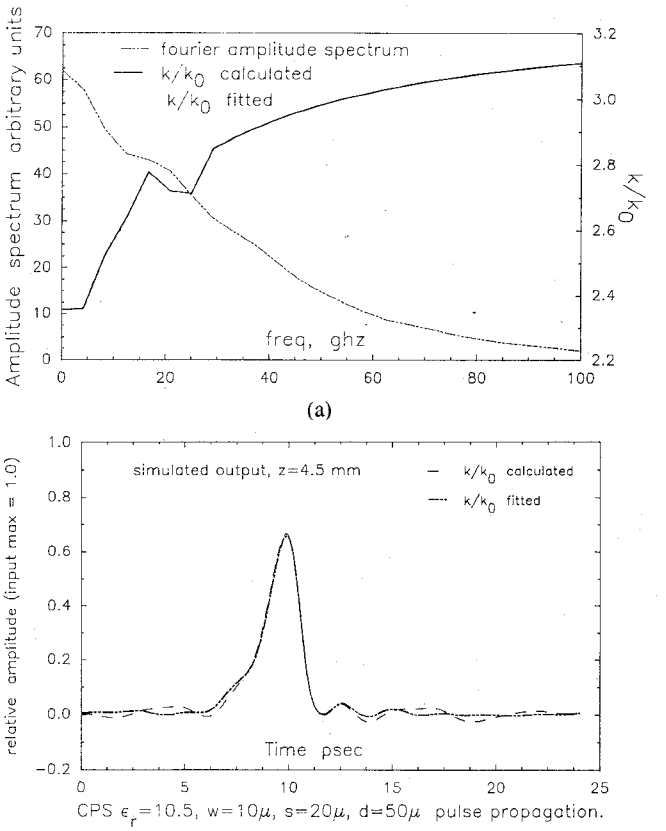

Fig. 7. Effect of the dispersion peak on pulse propagation. The CPS dimensions are $w = 10\ \mu$m, $s = 20\ \mu$m, and $d = 50\ \mu$m. (a) Fourier amplitude spectrum of the input pulse, the actual, and fitted dispersion curve, plotted versus the same frequency scale. (b) Simulated output pulses at a distance $z = 4.5$ mm with and without the dispersion peak included in the calculation.

dimensions that give rise to a strong peak in the dispersion curve. The input pulse waveform is the same as that in Fig. 4(a). The pulse duration is such that the frequency component in the transform which corresponds to the strong dispersion peak has a significant amplitude compared to the maximum. The transform of the input pulse is plotted along with the waveguide dispersion in Fig. 7(a). Fig. 7(b) shows the simulated output, once with the dispersion peak included and then with the peak excluded and the actual dispersion curve replaced by the smoothed curve fitted as per (2) and (3). There is more ringing in the calculation which includes peaks than with the smoothed curve. In this simulation, only one peak of the dispersion curve was included to isolate its effect on the propagated waveform. In reality, however, more peaks are present in the dispersion curve when more than one substrate mode is excited. These additional peaks can lead to more spread and ringing in the output.

IV. Conclusion

This analysis shows that substrate losses dominate pulse propagation and must be incorporated along with dispersion peaks, modal dispersion, and other relevant phenomena in the pulse propagation model. Conductor and dielectric losses are not estimated very accurately, but it is evident that these losses contribute little to the total loss, particularly at high frequencies. The onset and coupling of the substrate modes to the transmission line mode lead to the peaks in the dispersion curve. This can deteriorate pulses on propagation. Coplanar stripline parameters obtained by full-wave analysis agree well with results of established theory and data and indicate that lines can be closely placed with little interference if the surface wave losses can be eliminated. Field estimates also help evaluate optimal distances and dimensions for electro-optic sampling gaps, probes, and other experimental apparatus. The pulse propagation results also imply that superconducting phenomena are not the dominant mechanisms. Hence, curtailing radiation losses by using very thin substrates or other means will yield a larger improvement in pulse propagation performance than superconducting lines alone.

Acknowledgment

The authors wish to thank Dr. N. K. Das for stimulating discussions and C. Lutz for a critical review of the manuscript. They also thank D. Vassilovski and other members of their research group for their help.

References

[1] K. K. Li, G. Arjavalingam, A. Dines, and J. R. Whinery, "Propagation of picosecond pulses on microwave striplines," *IEEE Trans. Microwave Theory Tech.*, vol. MTT-30, pp. 1270–1273, Aug. 1982.

[2] G. Hasnain, A. Dines, and J. R. Whinery, "Dispersion of picosecond pulses in coplanar transmission lines," *IEEE Trans. Microwave Theory Tech.*, vol. MTT-34, pp. 738–741, June 1986.

[3] G. A. Mourou and K. E. Meyer, "Subpicosecond electro-optic sampling using coplanar strip transmission lines," *Appl. Phys. Lett.*, vol. 45, pp. 492–494, Sept. 1984.
[4] M. B. Ketchen *et al.*, "Generation of subpicosecond electrical pulses on coplanar transmission lines," *Appl. Phys. Lett.*, vol. 48, pp. 751–753, Mar. 1986.
[5] C. C. Chi *et al.*, "Subpicosecond optoelectronic study of superconducting transmission lines," *IEEE Trans. Magn.*, vol. MAG-23, pp. 1666–1669, Mar. 1987.
[6] D. R. Dykaar *et al.*, "Propagation characteristics of picosecond electrical transients on coplanar striplines," *Appl. Phys. Lett.*, vol. 51, pp. 1551–1553, Nov. 1987.
[7] J. F. Whitaker *et al.*, "Propagation model for ultrafast signals on superconducting dispersive striplines," *IEEE Trans. Microwave Theory Tech.*, vol. 36, pp. 277–285, Feb. 1988.
[8] D. P. Kasilingam and D. B. Rutledge, "Surface wave losses of coplanar transmission lines," in *IEEE MTT-S Int. Microwave Symp. Dig.*, 1983, pp. 113–116.
[9] D. B. Rutledge, D. P. Neikirk, and D. P. Kasilingam, *Planar Integrated Circuit Antennas*, vol. 10, *Millimeter Components and Techniques*, part II of *Infrared and Millimeter Waves*, K. J. Button, ed. New York: Academic Press, 1983, ch. 1.
[10] D. S. Phatak, N. K. Das, and A. P. Defonzo, "Dispersion characteristics of optically excited coplaner striplines: Comprehensive full wave analysis," to be published.
[11] M. Tsuji, H. Shigesawa, and A. A. Oliner, "Printed-circuit waveguides with anisotropic substrates: A new leakage effect," in *IEEE MTT-S Int. Microwave Symp. Dig.*, pp. 783–786, 1989,
[12] R. Mittra and T. Itoh, "A new technique for the analysis of the dispersion characteristics of microstrip lines," *IEEE Trans. Microwave Theory Tech.*, vol. MTT-19, pp. 47–56, 1971.
[13] T. Itoh and R. Mittra, "Spectral domain approach for calculating dispersion characteristics of microstrip lines," *IEEE Trans. Microwave Theory Tech.*, vol. MTT-21, pp. 496–499, 1973.
[14] W. J. Getsinger, "Microstrip dispersion model," *IEEE Trans. Microwave Theory Tech.*, vol. MTT-21, pp. 34–39, 1973.
[15] G. Kompa and R. Mehran, "Planer waveguide model for calculating microstrip components," *Electron Lett.*, vol. 11, pp. 459–460, 1975.
[16] E. Yamashita, K. Atsuki and T. Udea, "An approximate dispersion formula of microstrip lines for computer aided design of microwave integrated circuits," *IEEE Trans. Microwave Theory Tech.*, vol. MTT-27, pp. 1036–1038, Dec. 1979.
[17] K. C. Garg, K. C. Gupta and I. J. Bahl, *Microstrip Lines and Slotlines*. Dedham, MA: Artech House, 1979, ch. 7.
[18] N. K. Das and D. M. Pozar, "A generalized spectral domain Green's function for multilayer dielectric substrates with applications to multilayer transmission lines, *IEEE Trans. Microwave Theory Tech.*, vol. MTT-35, pp. 326–335, Mar. 1987.
[19] D. Grischkowsky, I. N. Duling III, J. C. Chen, and C. C. Chi, "Electromagnetic shock waves from transmission lines," *Phys. Rev. Lett.*, vol. 59, pp. 1663–1666, Oct. 1987.
[20] Ch. Fattinger and D. Grischkowsky, "Observation of Electromagnetic shock waves from moving surface dipoles," *Phys. Rev. Lett.*, vol. 62, pp. 2961–2964, Jun. 1989.
[21] M. C. Nuss *et al.*, "Propagation of terahertz bandwidth electrical pulses on $YBa_2Cu_3O_{7-\delta}$ transmission lines on lanthanum aluminate," *App. Phys. Lett.*, vol. 54, pp. 2265–2267, May 1989.

✠

D. S. Phatak, photograph and biography not available at the time of publication.

✠

A. P. Defonzo (SM'84), photograph and biography not available at the time of publication.